Electrical Engineering
https://doi.org/10.1007/s00202-024-02622-2

ORIGINAL PAPER

Enhanced supervisor energy management technique of DC microgrid-based PV/wind/battery/SC

Mohammed Abdulelah Albasheri[1] · Ouahid Bouchhida[1] · Youcef Soufi[2] · Abderrezzak Cherifi[3]

Received: 15 February 2024 / Accepted: 11 July 2024
© The Author(s), under exclusive licence to Springer-Verlag GmbH Germany, part of Springer Nature 2024

Abstract
Isolated DC microgrid-based renewable energy sources (RES) require a concurrent high energy and high-power density presence. The most effective approach is employing a hybrid energy storage system (HESS). Supercapacitors (SCs) are used to recover braking energy during fast power changes to improve battery performance and decrease battery stress. Additionally, SCs can be utilized to keep batteries charged for prolonged periods and store surplus energy generated by RES. This paper suggests an energy management technique EMT to facilitate energy sharing among RES, HESS, and the demand load. The EMT ensures that the state of charge SOC of the HESS remains within the limitation range ($80\% \geq \text{SOC} \geq 20\%$). Furthermore, the EMT regulates the DC link voltage and tracks the battery and SC with desired current references in twelve different scenarios. The effectiveness of the suggested EMT is verified through simulated tests performed under various fluctuations and operating situations. The EMT demonstrates successful power sharing among the components and achieves faster DC link voltage regulation with less than 2% overshoot. Moreover, the EMT enhances power quality attributes in the DC microgrid and enables smooth mode transitions.

Keywords Photovoltaic · DC microgrid · Renewable energy · Hybrid storage · Energy management · State of charge

Abbreviations

PV	Photovoltaic
SOC	State of charge
MPPT	Maximum power point tracking
EMT	Energy management technique
SC	Supercapacitor
HESS	Hybrid energy storage system
PMSG	Permanent magnet synchronous generator
MG	Microgrid
DCMG	Direct current microgrid
RESs	Renewable energy sources
ESS	Energy storage system
DC	Direct current
LPF	Low pass filter
PWM	Pulse width modulation
LPT	Load power tracking
LPS	Load power shedding

List of symbols

P	Power (w)
d	Duty ratio
PI	Proportional integral controller
s	Laplace operator
V_{DC}	Dc link voltage (v)
V_{ref}	Dc bus reference voltage (v)
SW	Converter switch
T	Temperature (°C)

✉ Mohammed Abdulelah Albasheri
Albasheri.mohamed@univ-medea.dz

Ouahid Bouchhida
bouahid2000@yahoo.fr

Youcef Soufi
youcef.soufi@univ-tebessa.dz

Abderrezzak Cherifi
Abderrezzak.cherifi@uvsq.fr

[1] Laboratoire de Recherche en Electrotechnique et Automatique, Departement of Technlogy, University of Médéa, Médéa, Algeria

[2] Laboratoire du génie Electrique-Labget, Departement of Electrical Engineering, University Echahid Larbi Tebessi, Tébessa, Algeria

[3] IUT de Mantes-en-Yvelines, Laboratoire END-ICAP - UMR 1179, Université Paris Saclay-Versailles, Versailles, France

Published online: 02 August 2024

E	Irradiance (w/m^2)
f_{LPF}	Transfer of the low pass filter
T_{S}	Constant time (s)
Ψ_{PM}	Magnetic flux
L_{PV}, L_{Wind}	DC–DC converter inductance of the PV and wind (H)
I_{pv}	Photovoltaic current
V_{pv}	Photovoltaic voltage
p	Air density
V_{w}	Wind speed (w/m)
λ	Tip speed ratio
Q	Is the battery capacity (Ah)
υ_{B}	Battery voltage
υ_{SC}	SC voltage
L_{SC}, L_{B}	DC–DC converter inductance of the SC and battery (H)
Q	Battery capacity (Ah)
$\mathrm{SOC_{SC}}$	State of charge of SC (%)
$\mathrm{SOC_B}$	State of charge of battery (%)
$\mathrm{SOC_{Max}}$	State of charge maximum (%)
$\mathrm{SOC_{Min}}$	State of charge minimum (%)
$\mathrm{SOC_{HESS}}$	State of charge of HESS (%)
B	Exponential zone time constant inverse (Ah^{-1})
I_{wind}	Wind current (A)
C_{DC}	DC bus capacitor (F)
I_{DC}	Load current (A)
L_{B}	DC–DC converter inductance of the battery (H)
R_{L}	Resistance of the load (Ω)
V_{SC} Rated	Rated voltage of the SC
E_{SC}	SC energy storage capacity
$K_{\mathrm{P_{SC}}}$, $K_{\mathrm{I_{SC}}}$	Proportional and integral gains of the SC PI controller
$K_{\mathrm{P_B}}$, $K_{\mathrm{I_B}}$	Proportional and integral gains of the battery PI controller
$K_{\mathrm{P_{DC}}}$, $K_{\mathrm{I_{DC}}}$	Proportional and integral gains of the DC link PI controller
I_{ds}, I_{qs}	Direct and quadratic stator currents (A)
V_{ds}, V_{qs}	Direct and quadratic stator voltages (V)
R_{s}	Resistance of the stator winding (Ω)

1 Introduction

Renewable energy was covered 36 percent of the world's electricity needs in 2023 [1]. Globally, an estimated 407 GW and 117 GW of solar photovoltaic and wind energy capacity were added in 2023. According to 'The Renewables Global Status Report 2023 (REN21), the highest level ever. This is because renewable energy costs less to run and receives preferential access to electricity networks when there is little demand for electricity [2]. In recent years, researchers have shown great interest in DC microgrids [3, 4]. The nonlinear electrical characteristics of wind and photovoltaic solar power are very significant. It is also that the fluctuating operating conditions are linked to changing weather patterns [5]. Microgrid designs may be categorized as either alternative or direct current, the loads and electrical network benefit from each microgrid system in different aspects [6, 7]. DC microgrids offer several benefits over alternative microgrids, including fewer converters, improved efficiency and quality, decreased power losses, and easier controllability [8, 9]. Compared to AC microgrids, DC microgrids may supply the loads directly, eliminating the problems associated with harmonics and phase synchronization [10]. Because of the fickle nature of (RESs) and the increasing demand for electricity in remote locations, (RESs) cannot meet the power needs during the day-night [11], more energy storage system (ESS) are needed to meet the load requirement [12]. DC microgrids are heavily reliant on energy storage systems (ESSs) to maintain the continuity of power delivery to loads while using fluctuating power sources such as solar and wind energy [13, 14]

Batteries are the most common kind of energy storage used in an isolated mode system [15]. Due to their low power density, sluggish dynamic characteristics, and slow charge/discharge rates, batteries have a high energy density [16]. To counteract rapid fluctuations in power, the battery and supercapacitor (SC) combination is favored owing to its lower power density [17, 18]. The researchers in [19] have shown many possible designs of a battery-supercapacitor combination. The optimum option is a multiple converter design, which makes use of two bidirectional buck-boost converters that are independent of one another [20].

It is also essential to establish an intelligent energy management and control to maximize the usage and lifespan of energy storage devices. Several control techniques for managing the power in renewable energy resources, stability, and voltage regulation have been discussed in the literature [21–23]. Cooperative control, multi-mode control technique, Droop control, and intelligent control are all widely used control approaches [24–26]. In [27], Grid-connected and grid-off PV/battery systems may be managed from a single location using centralized power management systems. Low-bandwidth communication and decentralized average current shared control have been used in [28], a distributed hierarchical control scheme. In [29], The DC link voltage is controlled using a nonlinear sliding mode controller.

However, the controller is less sensitive to external disturbances and has issues in sensitivity and reliability. In [30], control-based backstepping for DC microgrids has been suggested. But, the impact of integrating numerous renewable sources into shared DC links has not investigated. In [31], concentrated on control solutions for a microgrid that

includes of PV system, wind energy, and hybrid storage system consists SC and batteries linked to AC and DC lines, while the method established an easy control technique for coordinating the flow of electricity among alternative energy sources and storage devices. However, did not take into account the internal power sharing among storage devices. Fuzzy logic control (FLC) may also be used to manage hybrid renewable energy sources including storage devices [32–34]. FLC was employed to ensure a specific power balance among wind turbines, PV system and energy storage system in [35].

According to the consideration of the control issue in the preceding context, this study provides a novel robust energy management and control method for a standalone hybrid system based on a supervisor energy management technique containing a wind energy system, solar connected to a battery system, an SC, and a DC load.

Significant contributions of the suggested energy management strategy (EMT) are the following:

- The suggested EMT aims to improve the stability of the DC link voltage in comparison to traditional control methods, specifically in terms of transient behavior such as overshoot, undershoot, and settling time.
- Use the suggested EMT to ensure balanced power among RESs, batteries, and SC under different scenarios.
- Rapid restoration of DC link voltage to the reference voltage and reduction of the overshoot.
- The operation of the battery and supercapacitor within their state of charge limitations.
- Selected the optimal control for each situation.

The details of this paper are described as follows: the structure and modeling of the component of the DC microgrid are discussed in Sect. 2; in Sect. 3, the suggestion EMT is presented, and the simulation results and conclusion are given in Sects. 4 and 5.

2 System configuration

Figure 1 illustrates the DC microgrid architecture that is combined with HESS. The photovoltaic (PV), wind, battery, and (SC) are linked to DC link via (DC–DC) bidirectional converters, in contrast, DC loads are directly connected. The solar panel is connected to the DC bus via a (DC–DC) boost converter, while the wind source is coupled to the DC bus by a three-phase diode rectifier and a (DC–DC) boost converter.

2.1 Modeling of PV

Several mathematical equations of solar panels have been created to reflect the nonlinear behavior caused by the semiconductor's connections at the center of their implementation. The following mode was used in this work [36, 37]:

$$I_{pv} = I_{ph} - I_0\left[exp\left(\frac{q\left(V_{pv} + R_s \cdot I_{pv}\right)}{AN_sKT}\right) - 1\right] - \frac{V_{pv} + R_s \cdot I_{pv}}{R_{sh}} \quad (1)$$

where T is the actual temperature of the photovoltaic cell (k), A is the leakage current of the diode, N_s is the number of PV cells connected in series. q is the electron charge, and K is the Boltzman constant ($1381*10^{-23}$ J/k).

2.2 Modeling of wind energy

Power is extracted from wind speed by a wind turbine attached to the shaft of PMSG. Wind speed is provided by the equation [38]:

$$P_t = \frac{1}{2}pAC_p(\lambda, \beta)\omega_w^3 \quad (2)$$

Wind turbines have a limited ability to convert a certain proportion of the wind energy they gather. The percentage mentioned is denoted as $C_p(\lambda, \beta)$ and is determined by the wind speed, turbine speed, and blade pitch angle β. p—Air density; Area swept by the rotor blades $A = \pi R2$ ω_w—wind speed;

The tip speed ratio is known as the following [39]:

$$\lambda = \frac{R * \omega_m}{\omega_w} \quad (3)$$

where ω_m—angular speed of turbine rotor, R—radius of the turbine blade.

The PMSG model was constructed in the synchronous rotating d-q reference frame, with the d-axis aligned with the direction of the permanent magnet flux vector, the mathematical equations governing the (PMSG) in this reference frame may be elucidated as follows [40].

$$\begin{aligned} V_{ds} &= R_s \cdot I_{ds} + \frac{d\Psi_{ds}}{dt} - W_e \cdot \Psi_{qs} \\ V_{qs} &= R_s \cdot I_{qs} + \frac{d\psi_{qs}}{dt} + W_e \cdot \Psi_{ds} \end{aligned} \quad (4)$$

$$\begin{aligned} \psi_{ds} &= L_d \cdot I_{ds} + \Psi_{PM} \\ \psi_{qs} &= L_q \cdot I_{qs} \end{aligned} \quad (5)$$

The variables V_{ds} and V_{qs} represent the d-q components of the stator voltage vector, whereas I_{ds} and I_{qs} represent the d-q components of the stator current vector. R_s refers to the resistance of the stator phase. ψ_{ds} and ψ_{qs} represent the d-q components of the stator flux vector. L_d and L_q are the direct and quadrature stator inductances. Ψ_{PM} denotes the flux generated by the permanent magnets.

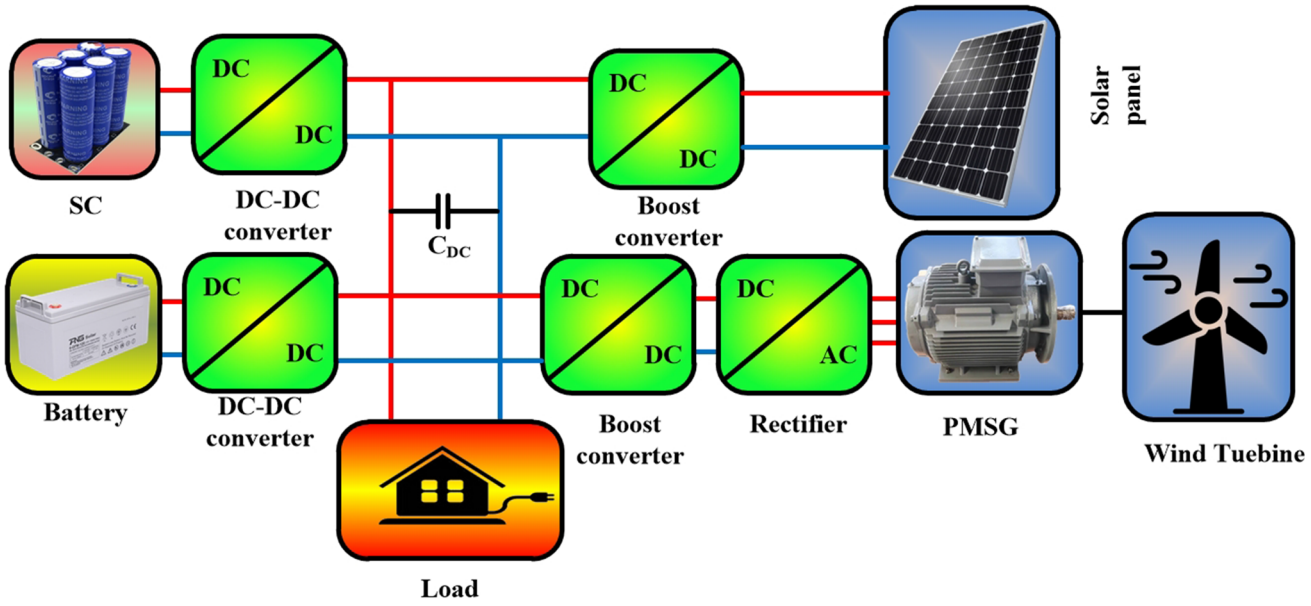


Fig. 1 Architecture of DC microgrid

2.3 Battery model

A battery cell uses electrochemistry to turn chemical energy into electrical energy. Compared to other energy storage devices, batteries used in green energy have a high energy efficiency, which is a benefit in remote area power system (REPS)-based microgrids use different kinds of batteries [41]. Battery is utilized in these applications because it works better than other types of (ESSs) [42]. The Simulink Simscape package developed the battery dynamic concept and is used in the tests in this work.

The voltage of battery, V_B may be expressed as follows [43]:

$$\mathbf{V_B} = \mathbf{E_0} - \mathbf{A_b e^{-(B.it)}} \frac{\mathbf{Q}}{\mathbf{Q - it}} \mathbf{I_{bat}} - \mathbf{R_b i} + \mathbf{A_b e^{-(B.I_{bat})}} - \mathbf{K} \frac{\mathbf{Q}}{\mathbf{Q - I_B}} \mathbf{I_B ref} \tag{6}$$

where R_b and B represent the exponential zone amplitude (V), and the exponential zone time constant inverse (Ah^{-1}), R_b is the battery internal resistance of (Ω), Q is the battery capacity (Ah), $I_B$ref is the battery reference current (A), I_B is the actual battery charge (A), and E_0 is the constant battery voltage (V).

2.4 SC model

SC has a high-power density, which can charge–discharge abruptly and swiftly, allowing it to absorb and supply a significant amount of power in a short period. The SC voltage and capacitance determine the SC energy storage capacity [44]:

$$\mathbf{E_{SC}} = \frac{\mathbf{C_{SC} v_{SC}^2}}{2} \tag{7}$$

Therefore, when the capacitor voltage varies, the energy stored changes proportionately, and the SOC_{SC} can be determined as:

$$\mathbf{SOC_{SC}} = \frac{\frac{\mathbf{C_{SC} v_{SC}^2}}{2}}{\frac{\mathbf{C_{SC} v_{SCRATED}^2}}{2}} \times 100\% = \left(\frac{\mathbf{v_{SC}}}{\mathbf{V_{SC}Rated}} \right)^2 \times 100\% \tag{8}$$

where the rated voltage of the SC is indicated by v_{SC}Rated.

2.5 Analysis of several HESS architectures built on supercapacitors and batteries

Numerous battery-SC HESS topologies have been proposed in different applications to maximize the advantage of HESS utilization. HESS designs can be classified based on the methods of linking to the DC link and used converters. HESS can be designed to be passive, active, or a mix of both in parallel or series [45], as illustrated in Fig. 2.

The connection of the ESS that is directly linked to the DC is known as passive structure. The power-sharing mechanisms and reaction are solely defined by the electrical characteristics of the ESS components, where SC operates as a low pass filter; because of the different terminal voltage characteristics of the battery and the SC, the capacity of the SC cannot be exploited entirely in passive HESS, due to the low volumetric efficiency and also flexibility in HESS architecture [45]. It is the first HESS architecture idea rarely employed in real-world applications in Fig. 2a, b.

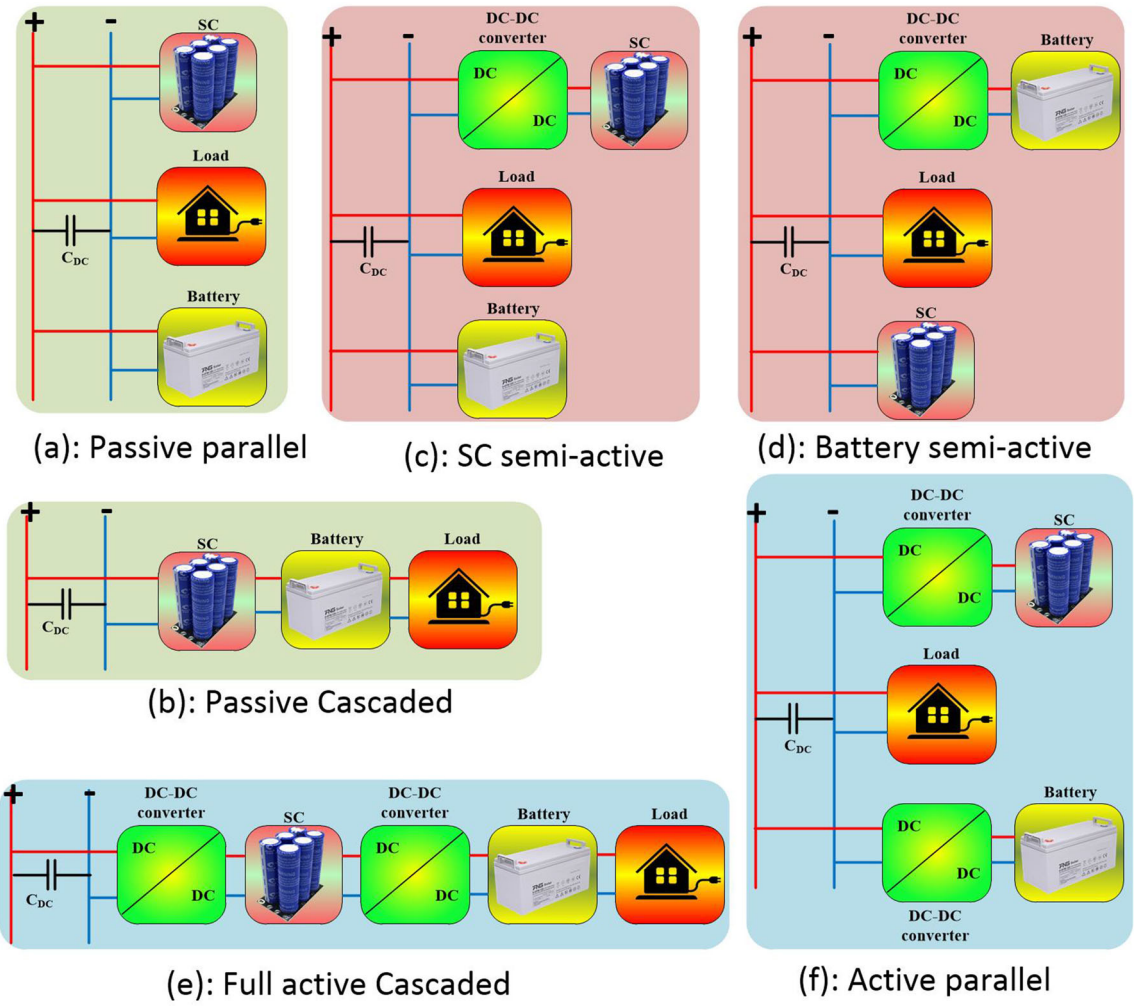


Fig. 2 HESS topologies classification

Semi-active HESS configurations, as depicted in Fig. 2c, d have been suggested to use the advantages, including both passive and active ESS configurations, while accounting for both disadvantages. The SC unit is regulated by a reversible DC/DC converter in SC semi-active HESS Fig. 2c, while the battery section is passively linked to the DC link. In the battery semi-active HESS design in Fig. 2d, SC section connects directly to the DC link and connects the battery unit with the bidirectional DC/DC converter [39]. Wide and unstable DC bus voltage is predicted due to the linear voltage-capacity nature, which might be a drawback in several systems. Nevertheless, the low volumetric efficiency of SC use is a critical flaw in this design. The SC system must be large enough to accommodate a broad range of DC link voltages. On the other hand, separating ESS elements using bidirectional DC/DC converters provides more flexible system configuration settings and active power flow management between ESS components.

The ESS units that are actively managed can be linked in cascaded Fig. 2e, or parallel Fig. 2f, the utterly active design can provide a significant level of control. Parallel active configuration is used in this work, as illustrated in Fig. 2f. The battery and SC voltages can be kept lower than the DC link, resulting in fewer balancing issues. The capacitor is thoroughly utilized because the SC's voltage might vary widely. This design allows battery and supercapacitor power to be managed separately based on their state of charge and supply requirements. The downside of this topology is the increased quantity and expense of components compared to previous designs.

3 Energy management control technique

The architecture of the DC microgrid, which has been given in this study, is shown in Fig. 1. The EMT described in this study is straightforward to configure and implement. When

the power generation cannot meet the demand or is greater than the power required, SC responds immediately and supports the excess or deficit power since the batteries cannot quickly compensate for the power change. As shown in the figure, the total current error, which represents the total current to be given by the HESS, is defined as the voltage error between the reference voltage and voltage measured, sent to the PI controller

$$\mathbf{\Delta I = I_{pv} + I_{wind} - I_{load} = I_{bat} + I_{sc}} \tag{9}$$

In this case, the current value ΔI^* is divided into two components: the high-frequency component fulfilled by the SC, and the low-frequency component fulfilled by the battery. Using a low pass filter permits the presence of the low-frequency component, which corresponds to the deficit reference current, as defined by the following equation:

$$\boldsymbol{\Delta I^* = f_{LPF}(\Delta I)} \tag{10}$$

When a charge limiter denotes the dynamic model of the low pass filter, it is formed to keep the batteries' reference current [46].

$$\mathbf{I}_{\text{bat_ ref}} = \boldsymbol{f}_{\mathbf{LPF}}\left(\mathbf{\Delta I}^*\right) \tag{11}$$

Reference value of battery is used to compare with measured value of battery. Then, the error is sent to this to the battery PI controller's, the control signal (d_B) generated by the PI control, the switches (Sb1, Sb2) are received pulses from the pulse width modulated (PWM) (Fig. 3).

The following fundamental goals are included in the design of the EMT:

- To ensure a balance of power in all operation modes.
- Improve DC link voltage stability, decrease the overshoot in transient period.
- Keep HESS SoC within acceptable limits and to avoid current oscillation of HESS at the edge of SoC limitation.
- To provide average power only over a lengthy period using a battery.
- SC produces oscillating and transient peak powers.

As illustrated in Fig. 4, there are twelve different modes to consider. Control techniques for controlling DC bus voltage throughout all operating states using storage devices or wind and PV solar are described below.

Maximum power point tracking (MPPT): using MPPT control when the Photovoltaic/wind power may be lower or greater than the load power demand while still maintaining limitations on the battery state of charge. As a result, the storage devices operating in charged/discharged scenarios.

Figure 3a depicts a schematic diagram of a typical controller design employed to accomplish the MPPT of a PV and wind energy integrated with a boost converter. Any voltage-based MPPT method may create the control loop reference voltage. The PV or wind energy readings are necessary for the MPPT algorithm (e.g., P&O) to work correctly.

Load power tracking (LPT): in this state, the wind and solar power are either greater than the load power, and the level of charge of the storage devices are full charged, in this control mode, the power produce by RESs follow the power load as reference power.

Load power shedding (LPS): In this case, the photovoltaic and wind power are much less than the load power, and the storage devices are entirely emptied. As a result, the loads are limited to the essentials, and the storage devices regulate the DC link voltage. In this case, the load decrease to the essential load.

- Design of PI controllers for DC bus voltage, SC, and battery

The DC link voltage is regulated by use a PI controller managed and controlled the transfer of energy between the various elements of the system by generated reference current $\boldsymbol{\Delta I^*}$. Determining the values of this controller is carried out by the DC–DC converters that are connected to HESS. In this model, a resistance is introduced in parallel with the load to reflect the various losses. The following are the formulas that will be used to design the suggested controller:

$$\boldsymbol{C_{dc}\frac{dV_{DC}}{dt} = I_{L_{SC}}d_{SC} - \frac{V_{DC}}{R_L} - I_{dc}} \tag{12}$$

$$\boldsymbol{L_{SC}\frac{dI_{SC}}{dt} = V_{SC} - d_{SC}V_{DC}} \tag{13}$$

The following dynamic expression could be constructed from the previously state formulas:

$$\boldsymbol{C_{dc}\frac{dV_{dc}}{dt} = I_{L_{SC}}\frac{V_{SC}}{V_{dc}} - \frac{V_{dc}}{R_L} - I_{dc}} \tag{14}$$

Using the Laplace domain as a model, that is possible to calculate the transfer function of a DC link.

$$\boldsymbol{FTx(s) = \frac{V_{DC(s)}}{I_{DC}(s)} = \frac{V_{SC}R_L}{\frac{R_L C_{SC}}{2}s + 1}} \tag{15}$$

Using the following expression, it can calculate the transfer function of the PI controller. That results in:

$$\boldsymbol{C_{DC}(s) = K_{P_{DC}} + \frac{K_{I_{DC}}}{s}} \tag{16}$$

Which results in:

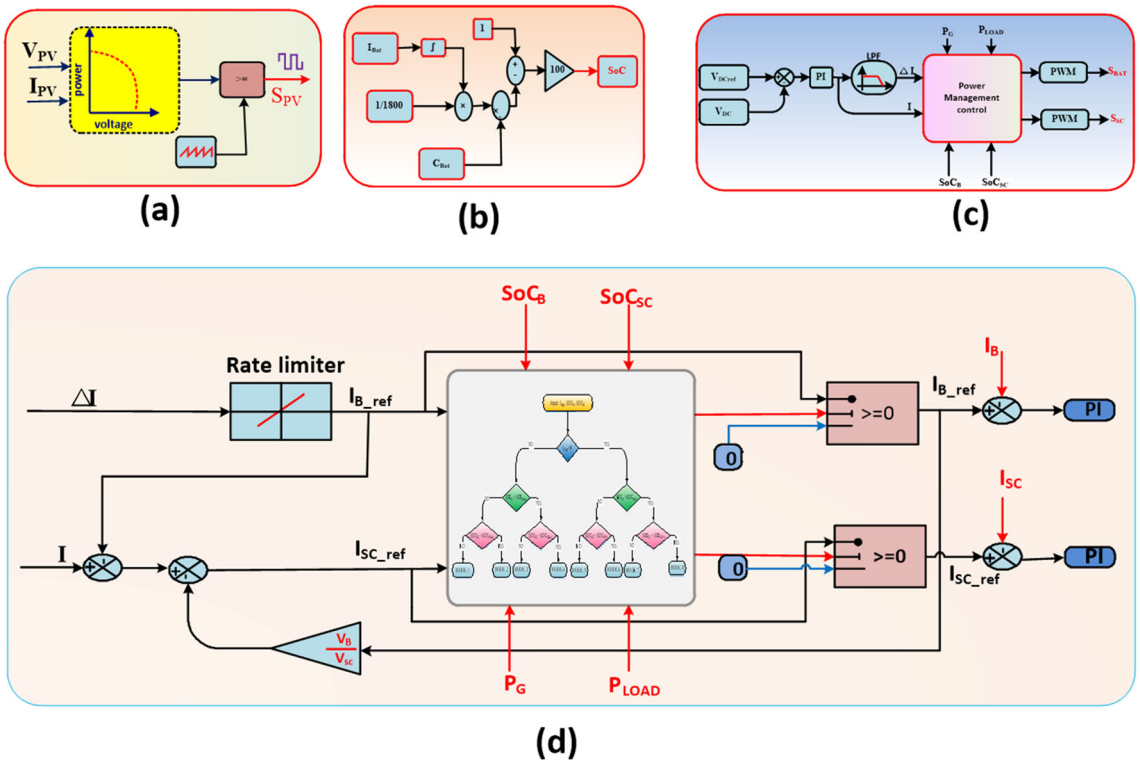


Fig. 3 **a** MPPT control, **b** battery SOC calculation, **c** energy management control, **d** control technique proposed

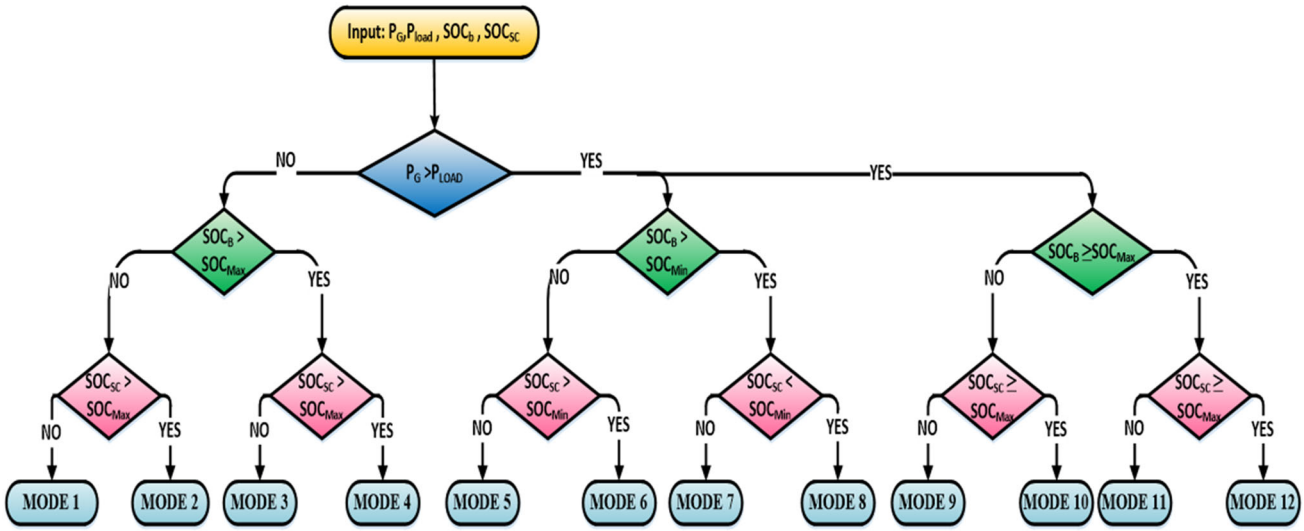
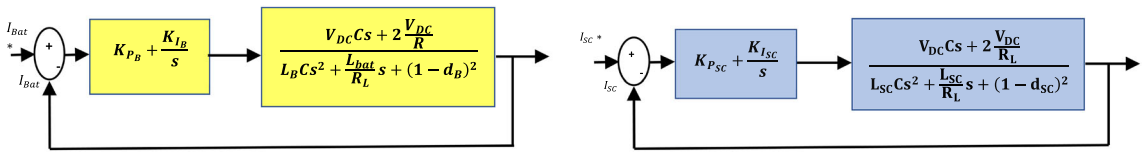


Fig. 4 Flow chart of power management proposed



(a): Block diagram of Battery controller. (b): Block diagram of SC controller

Fig. 5 **a** Block diagram of Battery controller. **b** Block diagram of SC controller

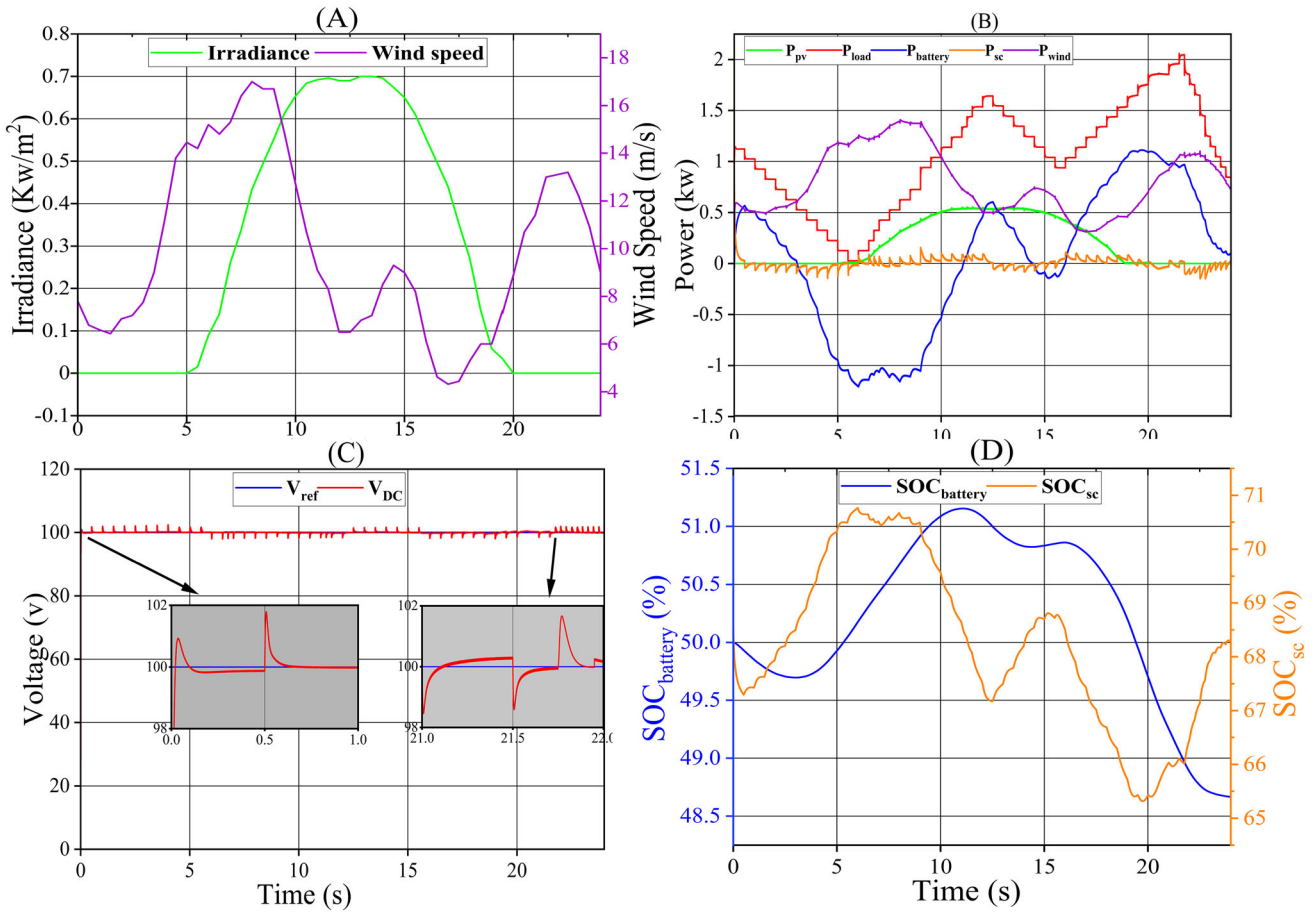


Fig. 6 **A** irradiation and wind speed profile, **B** power evaluations, **C** DC link voltage, **D** SOC_{HESS}

$$FTBF(s) = \frac{K_{P_{DC}} R_L V_{SC}\left(s + \frac{K_{i_{DC}}}{K_{p_{DC}}}\right)}{K_{p_{DC}} R_L V_{sC}\left(s + \frac{K_{I_{DC}}}{K_{p_{DC}}}\right) + s\left(\frac{R_L C_{SC}}{2} s + 1\right)} \tag{17}$$

The closed-loop Laplace transform is expressed by the following:

$$\mathbf{CLf(s)} = \frac{\frac{2}{C_{SC}} K_{p_{DC}} V_{SC}\left(s + \frac{K_{i_{dc}}}{K_{p_{DC}}}\right)}{s^2 + \frac{2}{\tau_L C_{SC}}\left(K_{p_{dc}} R_L V_{SC} + 1\right)s + \frac{2}{C_{SC}} V_{SC} K_{i_{DC}}} \tag{18}$$

We generate the denominator by associating it with the denominator of the canonical form.

$$\mathbf{And}\begin{cases} \omega_n^2 = \frac{2}{C_{SC}} V_{SC} K_{I_{DC}} \\ 2\xi\omega_n = \frac{2}{R_L C_{SC}}\left(K_{P_{DC}} R_L V_{SC} + 1\right) \end{cases} \tag{19}$$

$$\mathbf{Where}: \begin{cases} K_{P_{DC}} = \frac{\omega_n^2 C_{SC}}{2 V_{SC}} \\ K_{I_{DC}} = \frac{\omega_n^2 C_{SC}}{2 V_{SC}} \end{cases} \tag{20}$$

The bidirectional converter is controlled by the following expression, which may be written as (Fig. 5):

$$V_{SC} = L_{SC} \dot{i}_{L_{SC}}(s)s + R_{Load} i_{L_{SC}}(s) + (1 - D_{SC}(s))V_{dc} \tag{19}$$

As a result, the following expression is produced, which describes the relationship between the current and the duty ratio:

$$\frac{I_{SC}(s)}{d_{SC}(s)} = \frac{\frac{V_{DC}}{R_L}}{1 + \frac{L_{SC}}{R_L} s} \tag{21}$$

The corrector's transfer function is as described in the following:

$$G_{SC}(s) = \frac{K_{I_{SC}}\left(1 + \frac{K_{P_{SC}}}{K_{I_{SC}}}\right)}{s} \tag{22}$$

System transfer functions are simplified by considering a pole/zero and then applying to compensate: the transfer function changes to new form:

$$CLTF(s) = \frac{1}{1 + \frac{R_L}{V_{DC} K_{I_{SC}}} s} \tag{23}$$

where: $\tau_{SC} = \frac{R_L}{V_{dcDC} K_{I_{SC}}}$ is constant time of SC.

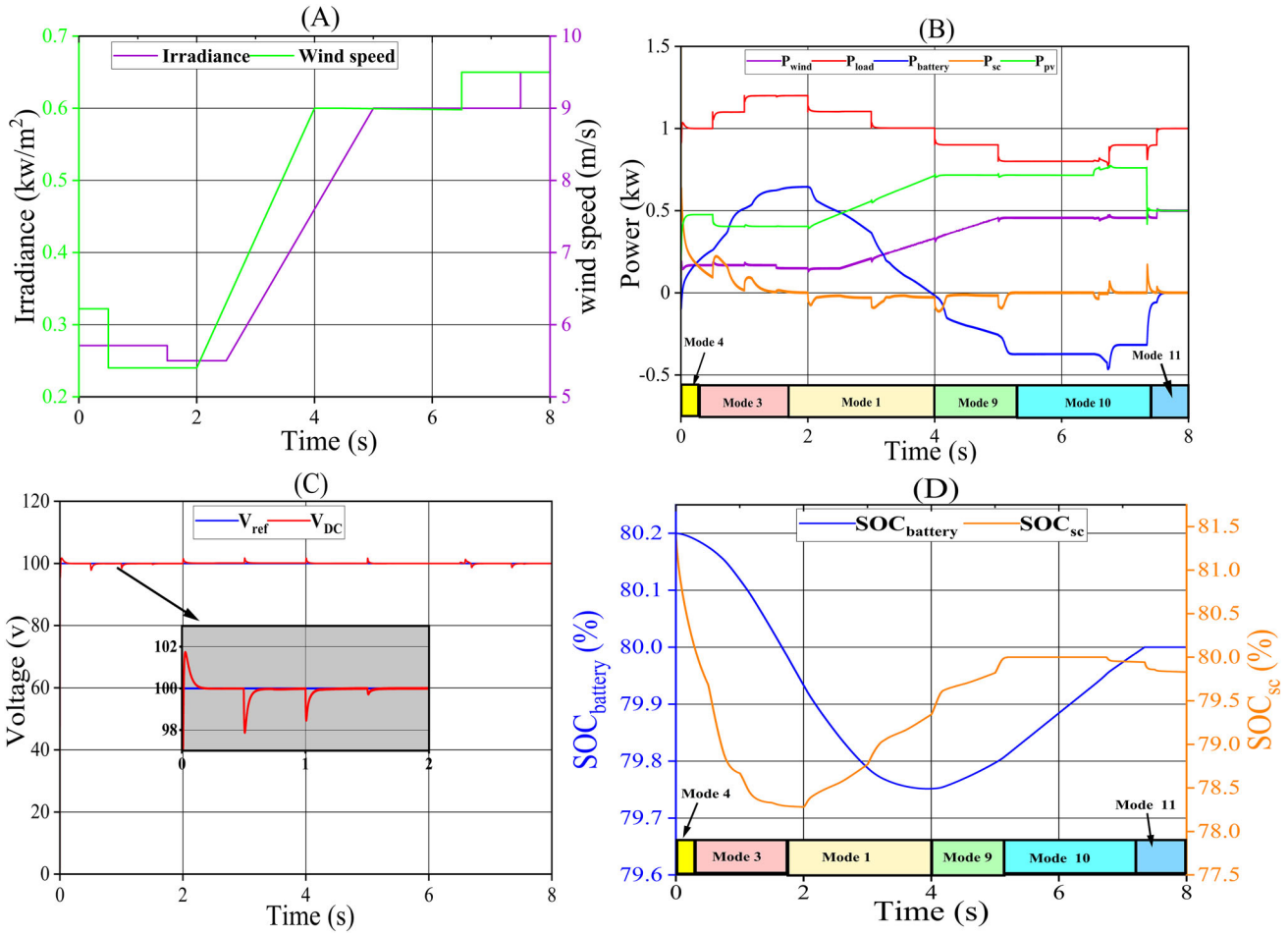


Fig. 7 **A** irradiation and wind speed profile, **B** power evaluations, **C** DC link voltage, **D** SOC_{HESS}

Consequently,

$$\mathbf{K_{I_{SC}}} = \frac{\mathbf{R_L}}{\boldsymbol{\tau}_{\mathbf{SC}}\mathbf{V_{DC}}} \text{ and } \mathbf{K_{P_{SC}}} = \frac{\mathbf{L_{SC}}}{\boldsymbol{\tau}_{\mathbf{SC}}\mathbf{V_{DC}}} \tag{24}$$

4 Simulation results

A simulation environment is used to test the viability of the suggested energy management plan. The purpose is to evaluate all feasible scenarios as well as do a one-day continuous test for the planned DC microgrid.

4.1 One-day experimental test

Unlike the next two experiments, which try to illustrate all different possibilities, the goal of the one-day experiment is to illustrate and verify the efficacy and implementation of the full system strategy in a real-life situation. As a result, no human intervention is required during the test. It is to validate that the hybrid battery/SC power system can perform well with the actual power (PV/Wind) and load profile under the direction of the suggested strategy. The data of irradiation and wind speed throughout the one-day test 0–24 obtained from a real location for a one-day dynamic tests, which was executed in October 2023 at Medea, Algeria. One second in the simulation study presented one hour in a real scenario. Figure 6A, depicts the actual sun light and air velocity on this day. Figure 6B, depicts the planned DC microgrid's power evolution over the course of one day. The load is provided by the battery and Wind power during the period (0–5) and (20–24). SCs respond immediately and quickly to the deficiency or surplus in situations of fluctuation in power generation or power load. The extra power generated by (PV/wind) is utilized to charge the batteries during the period (5–20). The waveform of the DC bus voltage is shown in Fig. 6C, which is maintained constant at 100v, there are slight fluctuations (fewer than 2% of the rated DC link voltage). Throughout the working range. The evolutions of SOC_{HESS} in Fig. 6D, indicate that storage capacities are

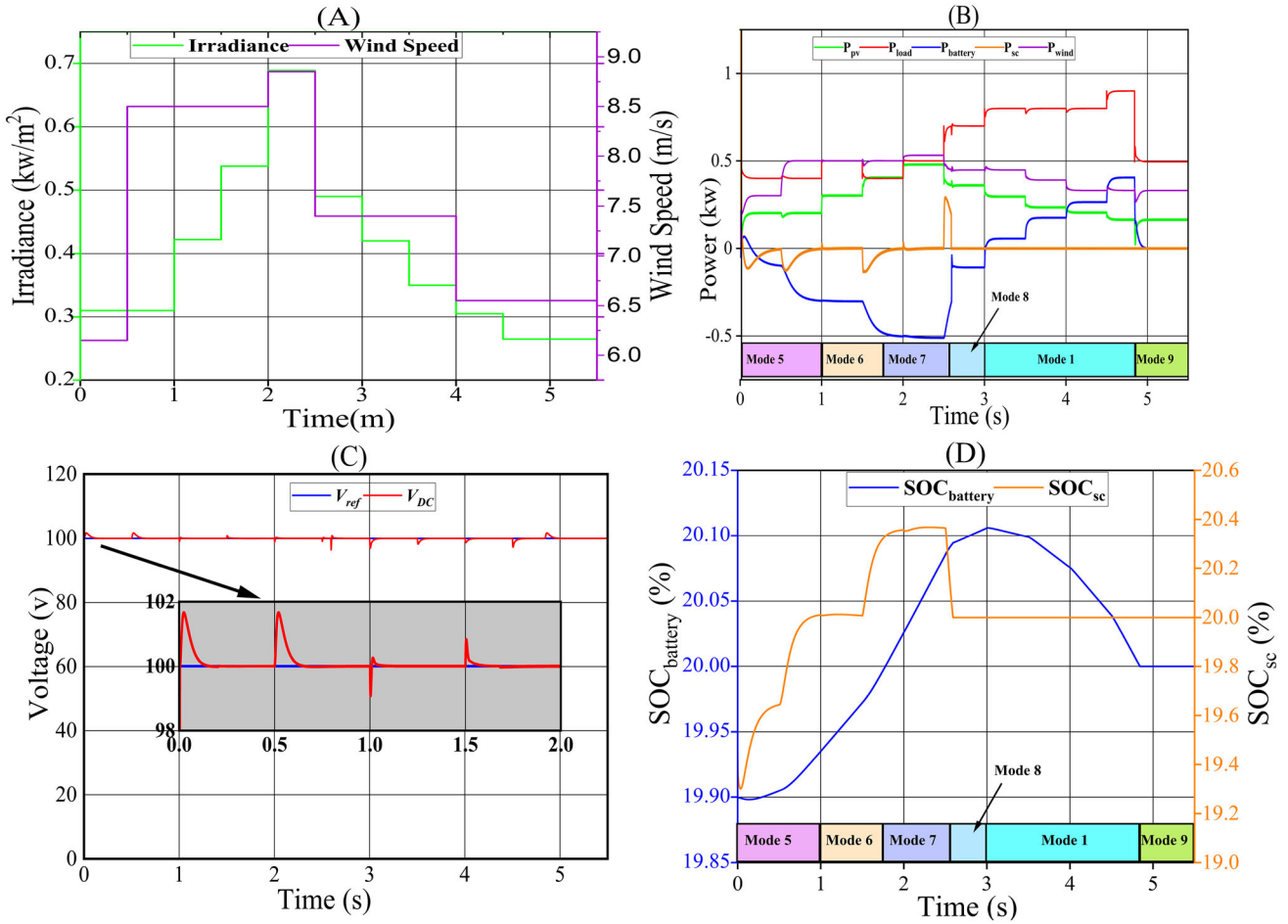


Fig. 8 **a** irradiation and wind speed profile, **b** power evaluations, **c** DC link voltage, **d** SOC_{HESS}

respected. Both supplying and absorbing energy, the battery and SC are effective.

4.2 HESS SOC upper limit situation

Figure 7A, demonstrates the variations in sunlight irradiation and wind velocity. Figure 7B, D, depict the operating results when the battery and SC are fully charged. In the first interval (mode 4), the power production is less than the power load, and SOC_B and SOC_{SC} are upper thanSOC_{Max}, the SC is discharged to compensate for the shortfall. Then, (mode 3), SC discharge to reach lower than SOC_{Max}. Similar in (mode 1), battery discharge to cover the deficit, SOC_B is lower than SOC_{Max}. In (mode 9), the power generation increased to be more than power load in this case the battery and SC absorbed the surplus power to reach at SOC_{Max}. Where the SC is fully charged and SOC_{SC} equally SOC_{Max} in (mode 10). After fully charge of SC the surplus power absorbed by the battery. As appear that the surplus or deficit power is absorbed and supplied by the battey and SC. Where (PV/wind) are operated in MPPT control to extract the maximum power. At the end in (mode 11) the HESS are fully charge. As a consequence, PV is converted from MPPT to LPT mode in order to share the load demand. In Fig. 7C., DC link voltage kept constant in followed the reference value 100v through all the modes.

4.3 HESS SOC lower limit situation

Figure 8A, demonstrates the variations in sunlight irradiation and wind velocity. In Fig. 8B, PV, wind, load, battery and SC power variations are shows, where the SOC_B and SOC_{SC} are illustrated in Fig. 8D.

The operation scenario is as follows: In (mode 5) the power produced from PV and wind are more than load required, the excess power is absorbed by battery and SC that their SOC are lower than SOC_{Min}. SOC_{SC} is rapidly charged to reach its SOC upper than SOC_{Min} in (mode 6). In (mode 7) battery is continuously charge to reach more then SOC_{Min}.

In the end of (mode 7), the power generation is decreased to be lower than the demand load in (mode 8), where the SC is supplied power deficit. In (mode 1), the power deficit is increased, this power is compensated by the battery. However, SOC_B is discharged to reach the SOC_{Min}, in (mode 9), where control mode switched from MPPT to LPS to reduce

the load to the essential load at 0.5 kw. Figure 8B demonstrates that the utilization of HESS in the system simulation effectively mitigates the adverse impact of peak currents on the batteries, and appears exponentially. SC additionally decrease the variation of the DC bus voltage when there are sudden changes in the load and variations in photovoltaic (PV) or wind power, as seen in Fig. 8C.

5 Conclusion

This study highlights the advantages of integrating hybrid energy storage devices to improve the stability, flexibility, and reliability of the DC microgrid. It achieves this by supporting intermittent renewable energy sources such as solar PV and wind energy. This study contributes to integrating three control modes (MPPT, LPT, and LPS) and developing an energy management technique to improve the performance of hybrid renewable energy systems (battery/SC). This research highlights the significance of choosing the optimal control mode. Moreover, the main features of the proposed EMT are reduced battery system stress, dynamic power distribution between the renewable energy sources (RESs) and storage devices, rapid restoration of DC link voltage, and the ability to keep the state of charge (SOC) of energy storage within the safe operating range. The suggested EMS was evaluated by employing simulation studies to validate its feasibility and efficiency. Using meteorological data, a one-day experiment was executed. Furthermore, two extreme scenarios are simulated to assess the efficiency of the system, when the SOC_B and SOC_{SC} are at or close to their maximum and lowest limits. The EMS successfully decreases power production, particularly during periods of excess power, (LPT), when SOC_B and SOC_{SC} is equal to or greater than SOC_{Max}. Similar, when the SOC_B and SOC_{SC}, optional (LPS) was used to prevent deep discharge.

Author contributions M.A.A. and O.B. wrote the main manuscript text Y.S. and A.C. reviewed the manuscript.

Data availability No datasets were generated or analysed during the current study.

Declarations

Competing interests The authors declare no competing interests.

References

1. "Renewable energy in energy supply | global trends". https://www.ren21.net/gsr-2024/. Accessed 28 Jun 2024
2. "IEA—International Energy Agency". IEA. https://www.iea.org. Accessed 28 Jun 2024
3. Yang Q, Jiang L, Zhao H, Zeng H (2018) Autonomous voltage regulation and current sharing in islanded multi-inverter DC microgrid. IEEE Trans Smart Grid 9(6):6429–6437. https://doi.org/10.1109/TSG.2017.2712658
4. Herrera L, Zhang W, Wang J (2017) Stability analysis and controller design of DC microgrids with constant power loads. IEEE Trans Smart Grid 8(2):881–888. https://doi.org/10.1109/TSG.2015.2457909
5. Ongaro F, Saggini S, Mattavelli P (2012) Li-ion battery-supercapacitor hybrid storage system for a long lifetime, photovoltaic-based wireless sensor network. IEEE Trans Power Electron 27(9):3944–3952
6. Zolfaghari M, Gharehpetian GB, Shafie-khah M, Catalão JPS (2022) Comprehensive review on the strategies for controlling the interconnection of AC and DC microgrids. Int J Electr Power Energy Syst 136:107742. https://doi.org/10.1016/j.ijepes.2021.107742
7. Planas E, Andreu J, Gárate JI, Martínez de Alegría I, Ibarra E (2015) AC and DC technology in microgrids: a review. Renew Sustain Energy Rev 43:726–749. https://doi.org/10.1016/j.rser.2014.11.067
8. Meng L et al (2017) Review on control of DC microgrids and multiple microgrid clusters. IEEE J Emerg Sel Top Power Electron 5(3):928–948. https://doi.org/10.1109/JESTPE.2017.2690219
9. Justo JJ, Mwasilu F, Lee J, Jung J-W (2013) AC-microgrids versus DC-microgrids with distributed energy resources: a review. Renew Sustain Energy Rev 24:387–405. https://doi.org/10.1016/j.rser.2013.03.067
10. Sanjeev P, Padhy NP, Agarwal P (2018) Peak energy management using renewable integrated DC microgrid. IEEE Trans Smart Grid 9(5):4906–4917. https://doi.org/10.1109/TSG.2017.2675917
11. Argyrou MC, Christodoulides P, Marouchos CC, Kalogirou SA (2018) Hybrid battery-supercapacitor mathematical modeling for PV application using Matlab/Simulink. In: 2018 53rd international universities power engineering conference (UPEC), pp 1–6. https://doi.org/10.1109/UPEC.2018.8541933
12. Argyrou MC, Christodoulides P, Marouchos CC, Kalogirou SA (2018) Hybrid battery-supercapacitor mathematical modeling for PV application using Matlab/Simulink. In: 2018 53rd international universities power engineering conference (UPEC). IEEE, Glasgow, pp 1–6. https://doi.org/10.1109/UPEC.2018.8541933
13. Benson CL, Magee CL (2014) On improvement rates for renewable energy technologies: solar PV, wind turbines, capacitors, and batteries. Renew Energy 68:745–751. https://doi.org/10.1016/j.renene.2014.03.002
14. Atia R, Yamada N (2016) Sizing and analysis of renewable energy and battery systems in residential microgrids. IEEE Trans Smart Grid 7(3):1204–1213. https://doi.org/10.1109/TSG.2016.2519541
15. Mendis N, Perera S (2014) Management of battery-supercapacitor hybrid energy storage and synchronous condenser for isolated operation of PMSG Based variable-speed wind turbine generating systems. IEEE Trans Smart Grid 5(2):10
16. Mendis N, Muttaqi KM, Perera S (2014) Management of low- and high-frequency power components in demand-generation fluctuations of a DFIG-based wind-dominated RAPS system using hybrid energy storage. IEEE Trans Ind Appl 50(3):2258–2268. https://doi.org/10.1109/TIA.2013.2289973
17. Thomas T, Mishra MK (2019) Control strategy for a PV-wind based standalone DC microgrid with hybrid energy storage system. In: 2019 IEEE 1st international conference on energy, systems and information processing (ICESIP), pp 1–6. https://doi.org/10.1109/ICESIP46348.2019.8938310
18. Mansir N, Taufiq-Yap YH, Rashid U, Lokman IM (2017) Investigation of heterogeneous solid acid catalyst performance on low grade feedstocks for biodiesel production: a review. Energy Convers Manag 141:171–182. https://doi.org/10.1016/j.enconman.2016.07.037

19. Laldin O, Moshirvaziri M, Trescases O (2013) Predictive algorithm for optimizing power flow in hybrid ultracapacitor/battery storage systems for light electric vehicles. IEEE Trans Power Electron 28(8):3882–3895. https://doi.org/10.1109/TPEL.2012.2226474
20. García P, Torreglosa JP, Fernández LM, Jurado F (2012) Viability study of a FC-battery-SC tramway controlled by equivalent consumption minimization strategy. Int J Hydrog Energy 37(11):9368–9382. https://doi.org/10.1016/j.ijhydene.2012.02.184
21. Singh P, Lather JS (2021) Power management and control of a grid-independent DC microgrid with hybrid energy storage system. Sustain Energy Technol Assess 43:100924. https://doi.org/10.1016/j.seta.2020.100924
22. Iovine A, Rigaut T, Damm G, De Santis E, Di Benedetto MD (2019) Power management for a DC MicroGrid integrating renewables and storages. Control Eng Pract 85:59–79. https://doi.org/10.1016/j.conengprac.2019.01.009
23. Sinha S, Bajpai P (2020) Power management of hybrid energy storage system in a standalone DC microgrid. J Energy Storage 30:101523. https://doi.org/10.1016/j.est.2020.101523
24. Diaz NL, Dragičević T, Vasquez JC, Guerrero JM (2014) Intelligent distributed generation and storage units for DC microgrids—a new concept on cooperative control without communications beyond droop control. IEEE Trans Smart Grid 5(5):2476–2485. https://doi.org/10.1109/TSG.2014.2341740
25. Fujita T, Yasuda T, Akagi H (2017) A dynamic wireless power transfer system applicable to a stationary system. IEEE Trans Ind Appl 53(4):3748–3757. https://doi.org/10.1109/TIA.2017.2680400
26. Ahn S-J, Park J-W, Chung I-Y, Moon S-I, Kang S-H, Nam S-R (2010) Power-sharing method of multiple distributed generators considering control modes and configurations of a microgrid. IEEE Trans Power Deliv 25(3):2007–2016. https://doi.org/10.1109/TPWRD.2010.2047736
27. Yi Z, Dong W, Etemadi AH (2018) A unified control and power management scheme for PV-battery-based hybrid microgrids for both grid-connected and islanded modes. IEEE Trans Smart Grid 9(6):5975–5985. https://doi.org/10.1109/TSG.2017.2700332
28. Anand S, Fernandes BG, Guerrero J (2013) Distributed control to ensure proportional load sharing and improve voltage regulation in low-voltage DC microgrids. IEEE Trans Power Electron 28(4):1900–1913. https://doi.org/10.1109/TPEL.2012.2215055
29. Cook MD, Parker GG, Robinett RD, Weaver WW (2017) Decentralized mode-adaptive guidance and control for DC microgrid. IEEE Trans Power Deliv 32(1):263–271. https://doi.org/10.1109/TPWRD.2016.2583384
30. Roy TK, Mahmud MA, Oo AMT, Haque ME, Muttaqi KM, Mendis N (2018) Nonlinear adaptive backstepping controller design for islanded DC microgrids. IEEE Trans Ind Appl 54(3):2857–2873. https://doi.org/10.1109/TIA.2018.2800680
31. Dong B, Li Y, Zheng Z, Xu L (2011) Control strategies of microgrid with hybrid DC and AC buses. In: Proceedings of the 2011 14th European conference on power electronics and applications, pp 1–8
32. Ben Salah C, Ouali M (2012) Energy management of a hybrid photovoltaic system. Int J Energy Res 36(1):130–138. https://doi.org/10.1002/er.1765
33. Kumar TP, Subrahmanyam N, Sydulu M (2022) Control strategies of a neuro-fuzzy controlled grid connected hybrid PV/PEMFC/battery. Glob J Res Eng. https://www.engineeringresearch.org/index.php/GJRE/article/view/1409. Accessed 15 Mar 2022
34. Li X, Hui D, Wu L, Lai X (2010) Control strategy of battery state of charge for wind/battery hybrid power system. In: 2010 IEEE international symposium on industrial electronics, pp 2723–2726. https://doi.org/10.1109/ISIE.2010.5637016
35. Badwawi RA, Abusara M, Mallick T (2015) A review of hybrid solar PV and wind energy system. Smart Sci 3(3):127–138. https://doi.org/10.1080/23080477.2015.11665647
36. Poshtkouhi S, Palaniappan V, Fard M, Trescases O (2012) A general approach for quantifying the benefit of distributed power electronics for fine grained MPPT in photovoltaic applications using 3-D modeling. IEEE Trans Power Electron 27(11):4656–4666. https://doi.org/10.1109/TPEL.2011.2173353
37. Rekioua D, Bensmail S, Bettar N (2014) Development of hybrid photovoltaic-fuel cell system for stand-alone application. Int J Hydrog Energy 39(3):1604–1611. https://doi.org/10.1016/j.ijhydene.2013.03.040
38. Tran D-H, Sareni B, Roboam X, Espanet C (2010) Integrated optimal design of a passive wind turbine system: an experimental validation. IEEE Trans Sustain Energy 1(1):48–56. https://doi.org/10.1109/TSTE.2010.2046685
39. Albasheri MA, Bouchhida O, Soufi Y, Moualdia A, Mujammal M (2022) Control and power management of DC microgrid based wind/battery/supercapacitor. In: 2022 IEEE 2nd international maghreb meeting of the conference on sciences and techniques of automatic control and computer engineering (MI-STA), pp 680–685. https://doi.org/10.1109/MI-STA54861.2022.9837665
40. Abdulelah AM, Ouahid B, Youcef S (2021) Control of a stand-alone variable speed wind turbine with a permanent magnet synchronous generator. In: 2021 18th international multi-conference on systems, signals devices (SSD), pp 546–550. https://doi.org/10.1109/SSD52085.2021.9429307
41. Zarate-Perez E, Santos-Mejía C, Sebastián R (2023) Reliability of autonomous solar-wind microgrids with battery energy storage system applied in the residential sector. Energy Rep 9:172–183. https://doi.org/10.1016/j.egyr.2023.05.239
42. Sreelekshmi SR, Lakshmi R, Nair MG (2022) AC microgrid with battery energy storage management under grid connected and islanded modes of operation. Energy Rep 8:350–357. https://doi.org/10.1016/j.egyr.2022.05.222
43. Rezk H, Nassef AM, Abdelkareem MA, Alami AH, Fathy A (2021) Comparison among various energy management strategies for reducing hydrogen consumption in a hybrid fuel cell/supercapacitor/battery system. Int J Hydrog Energy 46(8):6110–6126. https://doi.org/10.1016/j.ijhydene.2019.11.195
44. Yin C, Wu H, Locment F, Sechilariu M (2017) Energy management of DC microgrid based on photovoltaic combined with diesel generator and supercapacitor. Energy Convers Manag 132:14–27. https://doi.org/10.1016/j.enconman.2016.11.018
45. Cabrane Z, Ouassaid M, Maaroufi M (2016) Analysis and evaluation of battery-supercapacitor hybrid energy storage system for photovoltaic installation. Int J Hydrog Energy 41(45):20897–20907. https://doi.org/10.1016/j.ijhydene.2016.06.141
46. Al Basheri MA, Soufi Y, Bouchhida O, Cherifi A (2024) Control and energy management based on decoupling frequency of DC microgrid. In: 2024 21st international multi-conference on systems, signals & devices (SSD). IEEE, Erbil, pp 224–229. https://doi.org/10.1109/SSD61670.2024.10549218

Publisher's Note Springer Nature remains neutral with regard to jurisdictional claims in published maps and institutional affiliations.

Springer Nature or its licensor (e.g. a society or other partner) holds exclusive rights to this article under a publishing agreement with the author(s) or other rightsholder(s); author self-archiving of the accepted manuscript version of this article is solely governed by the terms of such publishing agreement and applicable law.